



Long-term corrosion behaviors of Hastelloy-N and Hastelloy-B3 in moisture-containing molten FLiNaK salt environments



Fan-Yi Ouyang*, Chi-Hung Chang, Ji-Jung Kai

Department of Engineering and System Science, National Tsing Hua University, Hsinchu 300, Taiwan, ROC

HIGHLIGHTS

- Corrosion behaviors of Hastelloy-N and -B3 in molten FLiNaK salt at 700 °C.
- The alleviated corrosion rate of alloys was observed after long-hour immersion.
- Long-term corrosion rate was limited by diffusion from matrix to alloy surface.
- Corrosion pattern transferred from intergranular corrosion into general corrosion.
- Presence of minor H₂O did not greatly influence the long-term corrosion behavior.

ARTICLE INFO

Article history:

Received 14 January 2013

Accepted 30 November 2013

Available online 6 December 2013

ABSTRACT

This study investigated long-term corrosion behaviors of Ni-based Hastelloy-N and Hastelloy-B3 under moisture-containing molten alkali fluoride salt (LiF–NaF–KF: 46.5–11.5–42%) environment at an ambient temperature of 700 °C. The Hastelloy-N and Hastelloy-B3 experienced similar weight losses for tested duration of 100–1000 h, which was caused by aggregate dissolution of Cr and Mo into FLiNaK salts. The corrosion rate of both alloys was high initially, but then reduced during the course of the test. The alleviated corrosion rate was due to the depletion of Cr and Mo near surface of the alloys and thus the long-term corrosion rate was controlled by diffusion of Cr and Mo outward to the alloy surface. The results of microstructural characterization revealed that the corrosion pattern for both alloys tended to be intergranular corrosion at early stage of corrosion test, and then transferred to general corrosion for longer immersion hours.

© 2013 Elsevier B.V. All rights reserved.

1. Introduction

A molten salt reactor (MSR) has been selected as one of next generation nuclear reactors, owing to its desirable properties of online refueling and burning of minor actinides in spent fuels, along with the capability with hydrogen production [1]. The MSR is designed to operate at high temperature for a higher thermodynamic efficiency and mainly uses molten salt mixtures as a coolant in the primary circuit; however, the molten salts intrinsically possess high corrosivity and cause the dissolution of materials. The corrosive environment will be aggravated when small amounts of impurities are present in the molten salts. The main impurities are oxides and hydroxide formed through molten salts contacting with H₂O and O₂ in air as well as the chemically reactive radioactive HF gas generated in the nuclear reactor core through the combination of hydrogen ion with fluoride ions during the operation of MSRs [2]. This corrosion issue may also degrade the mechanical behavior of the materials [3,4]. Therefore, the materials

required for usage in the MSR environment are expected to withstand high-temperature corrosion without degrading their mechanical strength for long-term severe operation conditions.

Hastelloy-N and similar Ni-based alloys are promising candidate material for MSR structure materials. Several literatures [5,6] have suggested that Hastelloy-N and similar alloys are resistant to corrosion at temperatures up to about 700 °C, but the developed passive oxide films (Al₂O₃, SiO₂, Cr₂O₃) on Hastelloy-N have been found to be chemically unstable and the strength of this alloy remarkably weakens under molten salt environments [7,8]. Olson et al. [5] investigated the corrosion behavior of Hastelloy-N, Hastelloy-X, Haynes-230, Inconel-617, and Incoloy-800H in molten salt environments at 850 °C for 500 h and indicated that corrosion mainly occurred at the grain boundaries of these alloys. They also revealed that original Cr-content of these alloys has pronounced influence on the corrosion rates [5]; higher original Cr-content would accelerate the corrosion rate of tested alloys. Furthermore, several researches [9–12] have also demonstrated that the corrosion behaviors are highly affected by the presence of impurity in the molten salts. Kondo et al. [9] pointed out that the corrosion rate of ferritic martensitic steel JLF-1 alloys may be

* Corresponding author. Tel.: +886 35715131x34321; fax: +886 35720724.

E-mail address: fyouyang@ess.nthu.edu.tw (F.-Y. Ouyang).

accelerated in the non-purified molten salt environment and corrosion mechanism of these tested alloys may change. Because the molten salts are difficult to be purified and tend to result in high water content in the salts, understanding how the moisture influences the long-term corrosion behaviors of Ni-based alloys is crucial. Therefore, this study investigated corrosion characteristics of Hastelloy-N and Hastelloy-B3 alloys in high-temperature molten alkali fluoride salt ($\text{LiF}-\text{NaF}-\text{KF}$) environments from 100 h up to 1000 h at an ambient temperature of 700 °C. To study how moisture affects the long-term corrosion behaviors of Ni-based alloys, the old FLiNaKs were replaced by the new one after each corrosion test. The results show that corrosion rates of the tested alloys were significant initially, and then reduced after long-hour immersion. The mechanism of alleviated corrosion rates was discussed and the corresponding microstructures of the corroded samples were also characterized.

2. Experimental

Two Ni-based Hastelloy-N (Haynes International, Inc.) and Hastelloy-B3 (Haynes International, Inc.) alloys having a dimension of $2 \text{ cm} \times 2 \text{ cm} \times 0.1 \text{ cm}$ were selected as the target materials for corrosion tests. The chemical composition of each alloy is listed in Table 1. Prior to corrosion tests, mechanical polishing was performed on the samples sequentially using SiC sandpapers of 800 and 1200 metallurgical grits and Al_2O_3 powders of $0.01 \mu\text{m}$. The samples were then ultrasonically cleaned in acetone and deionized water, respectively, for 5 min.

FLiNaK fluoride salts were chosen in this study owing to their better fluid transport and thermochemical properties as well as lower vapor pressures [2]. To maintain a lowest melting temperature of 454 °C [13], eutectic FLiNaK salts were composed of LiF (98%, FULLIN Chemical Co.), NaF (98.3%, SUNLIT FLUO & CHEMICAL CO.), and KF (98%, FULLIN Chemical Co.) at ratios of 46.5%, 11.5%, and 42%, respectively. Total weight of the molten salt powders ($\text{LiF } 410.2 \pm 1 \text{ g}$, $\text{NaF } 163.8 \pm 1 \text{ g}$, $\text{KF } 826 \pm 1 \text{ g}$) was approximately 1.4 kg. As the KF salt is hygroscopic, moisture inside the salts is

difficult to be completely removed. To minimize the moisture content in the FLiNaK salts, the FLiNaK salts were pre-heated in a furnace at 300 °C for 12 h in Ar gas environment, and then promptly poured into a pre-heated autoclave at 100 °C for subsequent corrosion tests. The corresponding moisture content in the FLiNaK salts was measured as 1.91 wt.% using Karl Fischer moisture analysis (MKC-520, Kyoto).

The experimental setup for corrosion test is represented schematically in Fig. 1. The setup consisted of a 2.5 L autoclave and an argon gas purging system. Because nickel has been proved to exhibit excellent corrosion resistance in the FLiNaK salts [6], the autoclave was made of alloy 625 with a pure nickel liner of 30 mm in thickness. A thermal couple, protected by a pure Ni sheath inside the autoclave, was used to measure the salt temperature. During the corrosion tests, the samples were immersed into the FLiNaK salts inside the autoclave and the salt temperature was set at 700 °C. Meanwhile, a dry Ar gas stream was introduced to maintain an inert surface environment for the molten salts and to carry possible gaseous HF away from the autoclave. To investigate how moisture affects long-term corrosion behaviors of the Ni-based alloys, the old FLiNaK salts were replaced by new one after a corrosion test of 100, 200, and 500 h. After tests, the retrieved samples were cleansed in 1 M $\text{Al}(\text{NO}_3)_3$ solutions (98.7%, J.T. Baker) to remove residual FLiNaK salts, following the method developed by Kirillov et al. [14]. After cleansing the samples, mass changes of the samples were measured using a high precision balance (accuracy $\pm 0.1 \text{ mg}$). Microstructural evolution and elemental composition of the samples were examined using scanning electron microscopy (SEM, JEOL JSM-6330-F, JEOL), transmission electron microscopy (FEG-HRTEM, JEOL JEM-2010F, JEOL) and energy dispersive X-ray analysis (EDX, JEOL JSM-6330-F, JEOL).

3. Results and discussion

Fig. 2 presents weight change of the samples after different immersion periods at 700 °C. The results show that the weight losses of both alloys increase with increasing immersion time.

Table 1
The compositions of Hastelloy-N and Hastelloy-B3 used in this study.

Alloy (wt.%)	Ni	Cr	Mo	Fe	W	Co	Mn	Al	Ti	Si	C	Others
Hastelloy-N	71	7	16	3	0.5	0.2	0.8			1	0.08	Al + Ti:0.35 Cu:0.35
Hastelloy-B3	65	1.5	28.5	1.5	3	3	3	0.5	0.2	0.1	0.01	

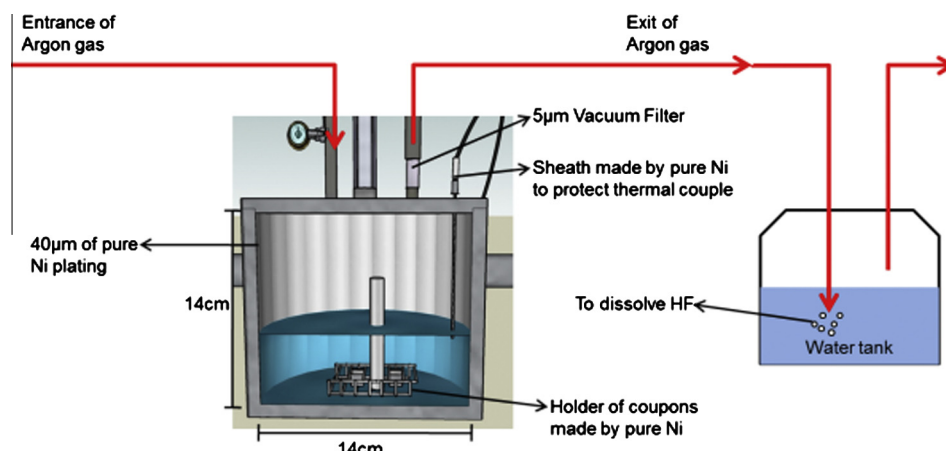


Fig. 1. Schematic diagram of experimental set up.

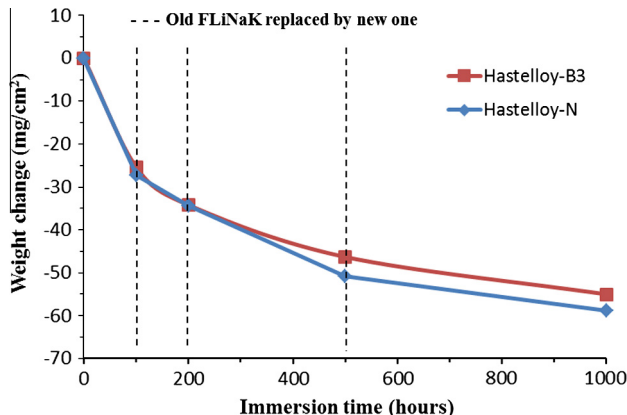


Fig. 2. The results of mass loss of Hastelloy-N and Hastelloy-B3 after different periods of corrosion tests.

We also find that Hastelloy-B3 experienced similar weight losses as Hastelloy-N at different immersion durations. When molten FLiNaK salts contain water, an HF gas would form at high temperature, resulted from the reactions of $MF_{(l)} + H_2O_{(g)} \rightarrow MOH_{(l)} + HF_{(g)}$ and $2MF_{(l)} + H_2O_{(g)} \rightarrow M_2O_{(l)} + 2HF_{(g)}$, where M represents K, Li and Na. Partial HF gas would dissolve into FLiNaK salts and corrode metal elements through the reaction $xMe + y HF_{(l)} \rightarrow Me_x F_y + y/2H_2(g)$, where Me represents the metal elements in the tested alloys [2]. Thus, for alloys tested in the moisture-containing molten salts environments, the tendency of metals to be corroded is mainly determined by thermodynamic driving force, i.e. difference in the free energy of HF and fluorides of the alloying element [3]. In other words, the alloys whose constituents have greater negative free energy to form metal fluoride are susceptible to corrosion. As shown in Table 2, because Cr possesses lower Gibbs free energy to form Cr fluorides, the Ni-based alloys containing lower Cr-contents are expected to exhibit better corrosion protection in the fluoride salt environments. Olsen et al. [5] have performed the corrosion tests in purified molten FLiNaK salts at 800 °C for 500 h in sealed graphite crucibles under Ar gas and indicated that weight losses of the tested alloys due to molten fluoride salt exposure generally increased as the initial Cr-contents of alloys increased. However, as evidenced in Table 1, the initial Cr-contents of Hastelloy-B3 was lower than that of Hastelloy-N by 5.5 wt.%, suggesting that the effect of initial Cr-content alone in the tested alloys failed to explain similar weight losses between Hastelloy-B3 and Hastelloy-N. We speculated that comparable weight losses of these two

tested alloys could be due to preferentially enhanced oxidation of Mo in the moisture-containing molten salts. Mo was easy to form MoO_3 as temperature is higher than 600 °C, thus higher moistures (impurities) inside the FLiNaK salts would result in a larger amount of MoO_3 . However, the oxide films of MoO_3 were chemically unstable in the FLiNaK salts and were easily to be dissolved into FLiNaK salts, finally leading to higher mass loss of tested alloys. Tyreman [17] have conducted a corrosion test for several pure metals, including Ni, Cu, Co, Fe, Cr, Mo, Nb and Ta, in a pure HF gas environment at 850 °C for 10 h and found that Mo was the most corrosion resistant material among all tested metals. However, when they repeated the corrosion test in a diluted 50% HF solution, corrosion rates of all materials decreased except for Mo. In fact, the corrosion rate of Mo increased by a factor of four. Thus, these data further support that Mo was involved in the corrosion reaction under moisture-containing molten salt environments. As shown in Table 1, Hastelloy-B3 had a relatively high Mo-content of 12.5 wt.% as compared with Hastelloy-N. Our previous study also indicated that mass losses of the tested alloys varied linearly with original Cr content plus one-third of Mo content (Cr wt.% + 1/3 Mo wt.%) when the moisture is present in the FLiNaK salts [18]. Therefore, aggregate dissolution of the Cr and Mo resulted in similar mass losses in these two alloys.

Fig. 3 shows corrosion rates of the tested alloys in terms of immersion times. The corrosion rates of each alloy were calculated according to net weight loss divided by the test interval. For example, the corrosion rate at 200 h was calculated based upon the mass loss between 100 h and 200 h. The result suggests that corrosion rates were relatively high at first 100 h and then decelerated rapidly at the following test hours. Similar phenomenon have been observed in Fe-based JLF-1 alloys (Fe-9Cr-2 W-0.1C) after corrosion test at 600 °C with 16.9 wt.% residual moisture in FLiNaK salts [9], indicating that the corrosion rate was reduced during the following 750 h when compared with that at first 250 h of corrosion test. The decreasing corrosion rate in Fe-based JLF-1 alloys at the chronic stage can be explained by alleviated impurities concentration. Because there are residual moisture existed in the FLiNaK salts, the initial corrosion reaction is expected to be fast and thus lead to higher mass losses. However, once the samples underwent long-hour immersion, the residual water in the molten salts and air impurities should be exhausted or expelled and sustained attack from those corrosion reactions will not occur. In other words, concentration of impurities in the FLiNaK salts decreased with increasing corrosion periods and in turn exhibited a relatively slower corrosion rate. However, reduced concentration of impurities in the molten salts seems to fail to explain the alleviated corrosion

Table 2
Free energy of formation of fluorides and oxides.

Fluoride/oxide	Temperature (K)	Free energy of formation (kJ/mole)	Reference
LiF	1000	-520.8	[15]
NaF	1000	-466.7	[15]
KF	1000	-454.2	[15]
HF	1000	-275.8	[15]
CrF ₂	1000	-313.3	[15]
MoF ₃	1000	-212.1	[15]
MoF ₆	1000	-209.2	[15]
FeF ₂	1000	-277.1	[15]
NiF ₂	1000	-230.4	[15]
WF ₆	1000	-236.7	[15]
Cr ₂ O ₃	1000	-861.6	[16]
MoO ₂	1000	-404.3	[16]
MoO ₃	1000	-486.9	[16]
Fe ₃ O ₄	1000	-780.8	[16]
Fe ₂ O ₃	1000	-556.8	[16]
NiO	1000	-150.7	[16]

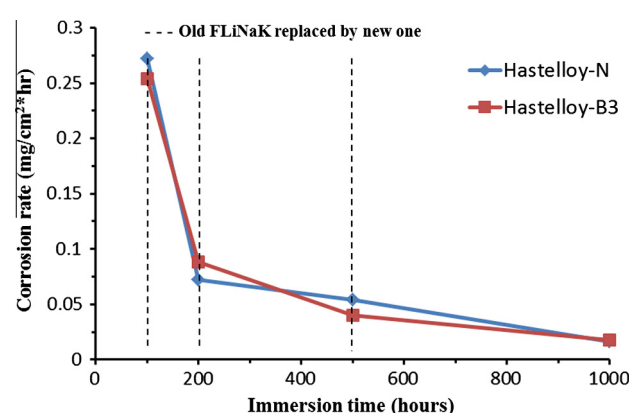


Fig. 3. Plot of corrosion rates of the Hastelloy-N and Hastelloy-B3 versus corrosion periods.

rate at the chronic stage in this study as the old FLiNaK salts were replaced by the new one after each test.

To understand the reason of alleviated corrosion rate at the chronic stage in this study, morphological SEM images of Hastelloy-N and Hastelloy-B3 after different periods of tests were examined, as shown in Fig. 4. At first 100 h and 200 h, corrosion occurred preferentially along grain boundaries and high-angle tilt boundaries for Hastelloy-N. It is believed that due to higher energy state of grain boundaries, grain boundaries are more chemically reactive than the grains themselves. In addition to intergranular corrosion, the relatively uniform reduction of thickness was also observed over the surface for Hastelloy-B3 at the early stage of tests. The difference of corrosion pattern between Hastelloy-N and Hastelloy-B3 at first 200 h is possibly due to a relatively larger amount of

Mo-content (20 wt.%) in the Hastelloy-B3 samples. It was reported that Ni-based alloys containing higher Mo contents would suffer more general corrosion than intergranular corrosion [19]. When the samples were tested for 500 h, it appeared that the dissolution of the alloy inside the grains became more outstanding for both Hastelloy-N and Hastelloy-B3, suggesting that corrosion pattern was transferring from intergranular corrosion into general corrosion. The effect of general corrosion was more pronounced after a test period of 1000 h, leading to approximately uniform corrosion across the entire surface area.

Fig. 5 shows the cross-sectional SEM images of Hastelloy-N after 1000 h of corrosion test. The corrosion pattern tended to be general corrosion, being consistent with what have been observed on the surface view. After immersing the samples in ASTM 66

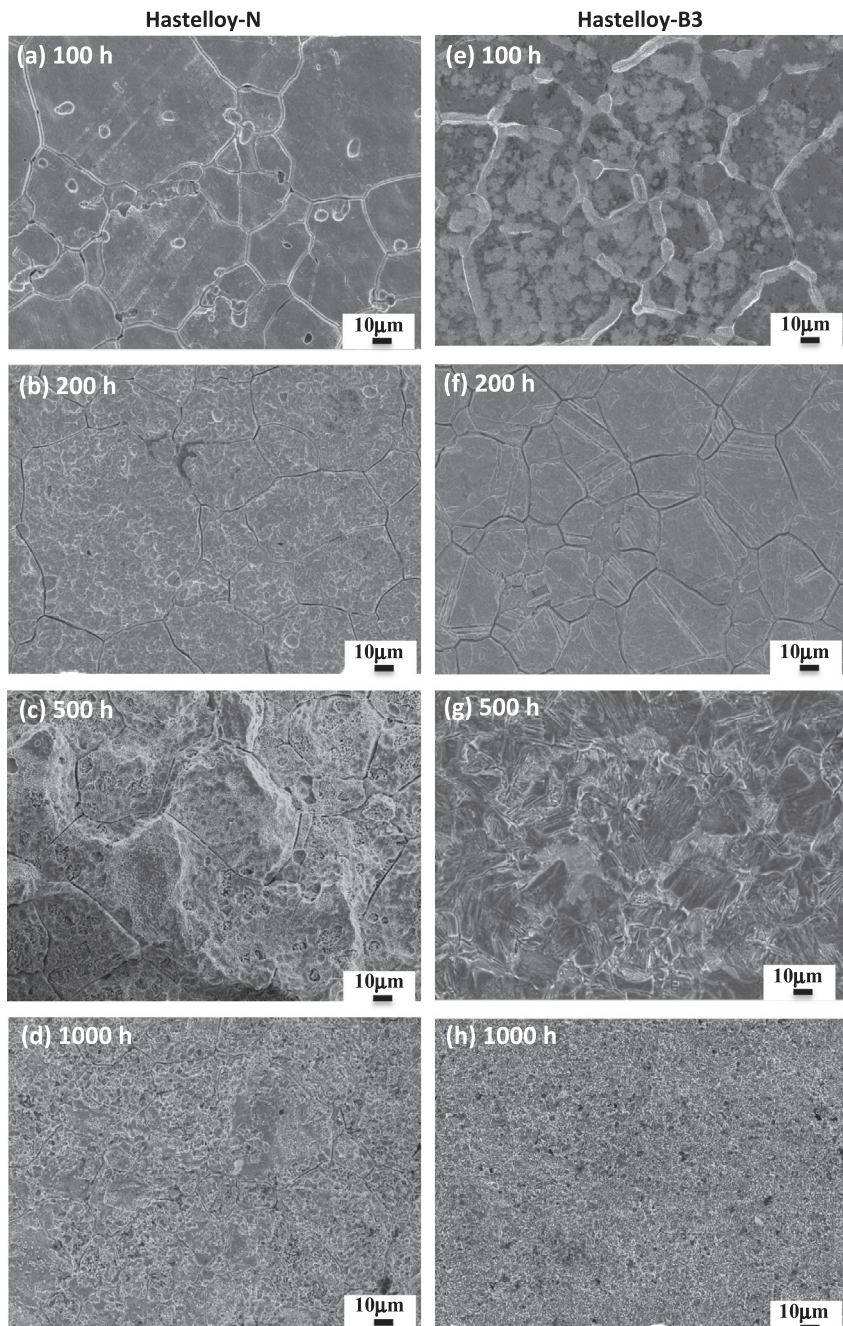


Fig. 4. The morphological SEM images of Hastelloy-N (with 7 wt.% Cr and 16 wt.% Mo) after (a) 100 h, (b) 200 h, (c) 500 h, and (d) 1000 h of corrosion tests, and Hastelloy-B3 (with 1.5 wt.% Cr and 28.5 wt.% Mo) after (e) 100 h, (f) 200 h, (g) 500 h, and (h) 1000 h of corrosion tests.

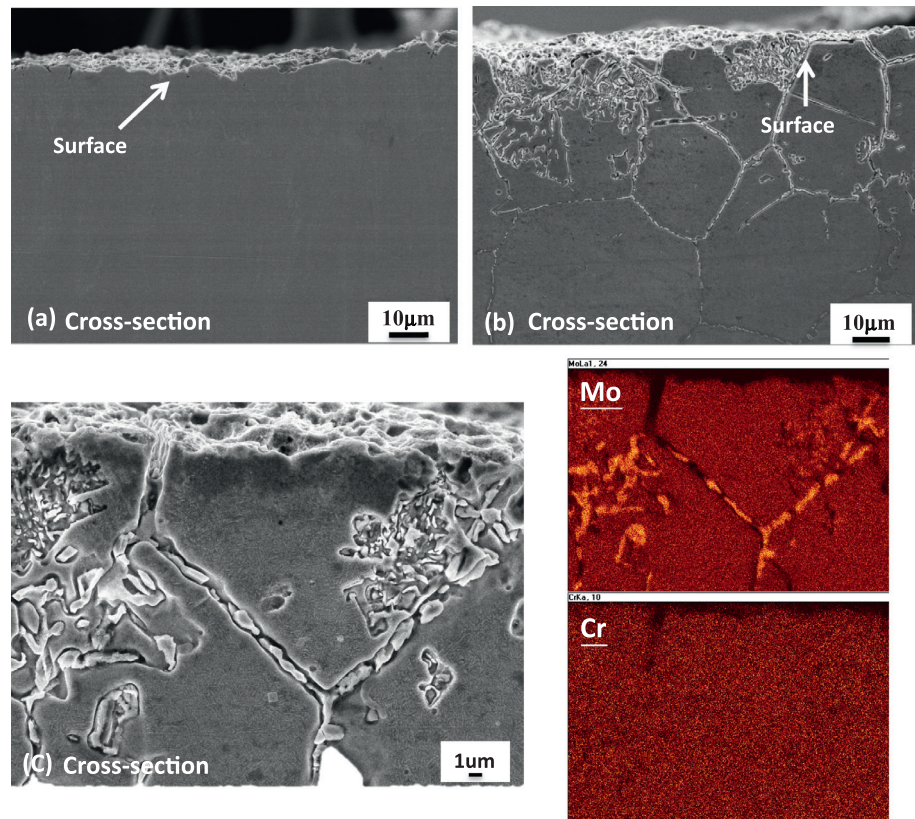


Fig. 5. The cross-sectional SEM images of Hastelloy-N (a) without and (b) with etching after 1000 h of corrosion test and (c) EDX mapping analysis on the cross-sectioned Hastelloy-N for Cr and Mo elements.

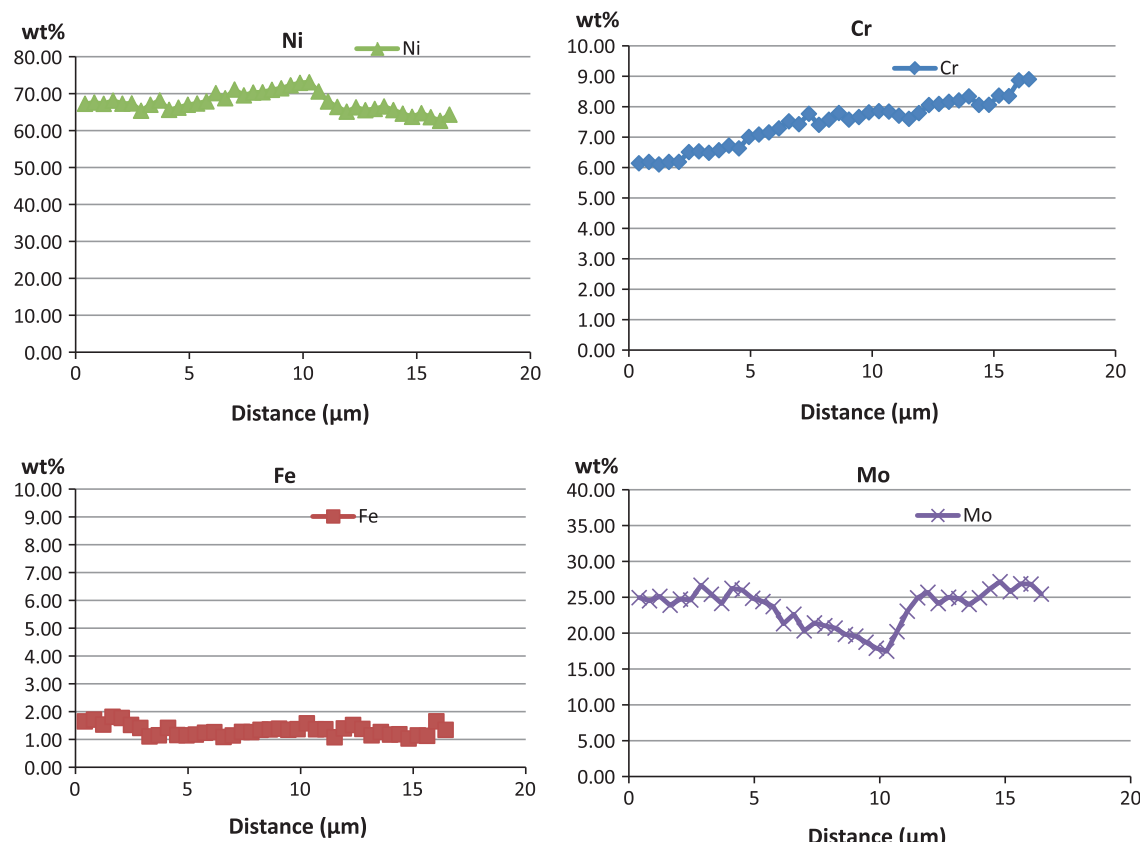


Fig. 6. Compositional distribution of Ni, Cr, Mo and Fe from surface toward the interior of Hastelloy-N after 1000 h of corrosion test.

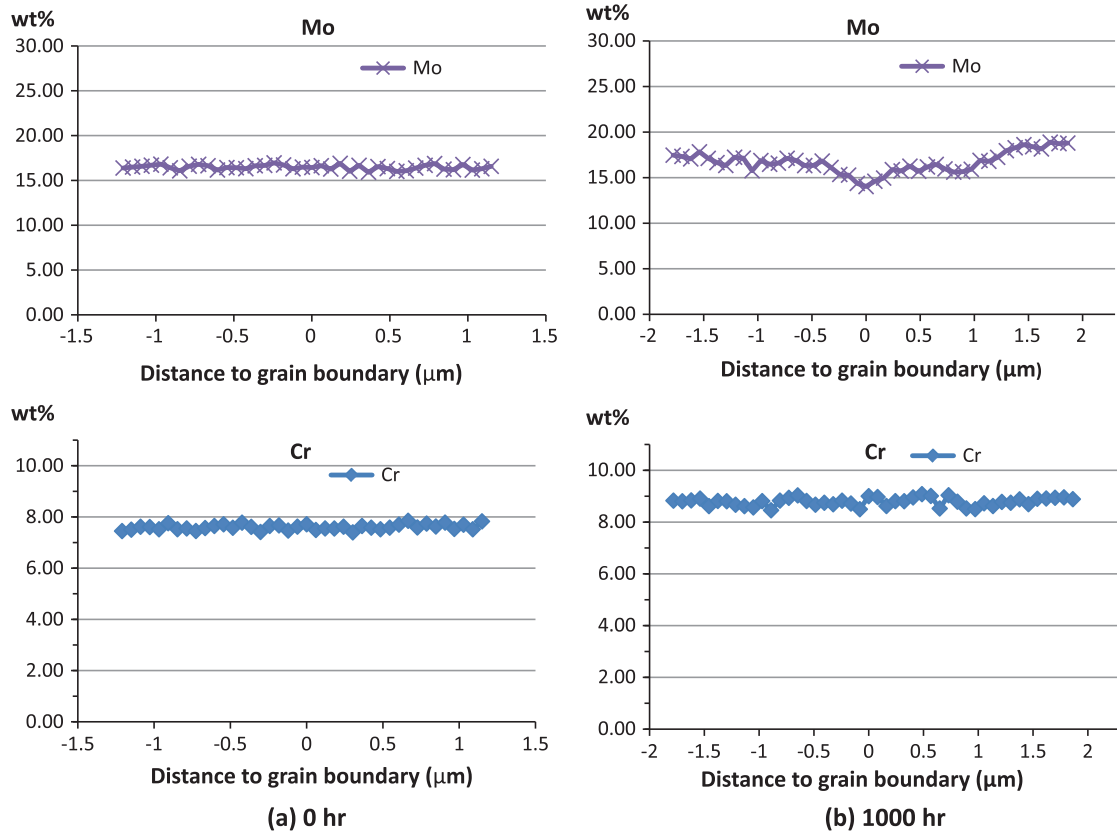


Fig. 7. Compositional distribution of Cr and Mo across grain boundaries of Hastelloy-N (a) before and (b) after 1000 h of corrosion test.

etchant for 3 s, we can find that some Mo-rich phases were formed at the grain boundary, as evidenced by EDX analysis in Fig. 5(c). TEM-EDX analysis performed on these precipitations confirms that the precipitations are M₆C-type carbides. Similar phenomenon was also observed by Gehlbach and McCoy [20], showing that M₆C-type carbides appeared in Hastelloy-N after exposure of the alloys to temperatures ranging from 500 °C to 1000 °C in an Ar atmosphere. Additionally, compositional distributions of Ni, Cr, Mo, and Fe atoms from the surface toward the interior region of cross-sectional Hastelloy-N after 1000 h of corrosion test are shown in Fig. 6. The results indicate that no significant variation of concentration of Ni and Fe were observed. However, there existed a Cr concentration gradient near the surface of the samples and a depletion region of Mo was observed in the depth of 10 μm. To confirm if the depletion of Cr and Mo was mainly caused by precipitation of carbides along grain boundary, Fig. 7(a) and (b) provides the compositional distribution of Cr and Mo across grain boundary before and after 1000 h of corrosion test, respectively. Interestingly, no significant depletion of Cr near the grain boundary was observed, inferring that the depletion zone of Cr observed near the surface of Hastelloy-N was not contributed from the precipitation of chromium carbide. Instead, these results suggest that the depletion zone near the surface was mainly caused by the dissolution of Cr into molten salt environment, which was consistent with the tendency regulated by the thermodynamic driving force. Additionally, the depletion of Mo was found near the grain boundary region, which supports that the depletion of Mo observed in Fig. 6 was mainly due to the formation of Mo-rich carbide in the grain boundary as shown in Fig. 5(c).

Fig. 8(a) and (b) shows the cross-sectional SEM image of Hastelloy-B3, containing most of Mo in addition to Ni, after 500 h and 1000 h of corrosion test, respectively. It is worth noting that two

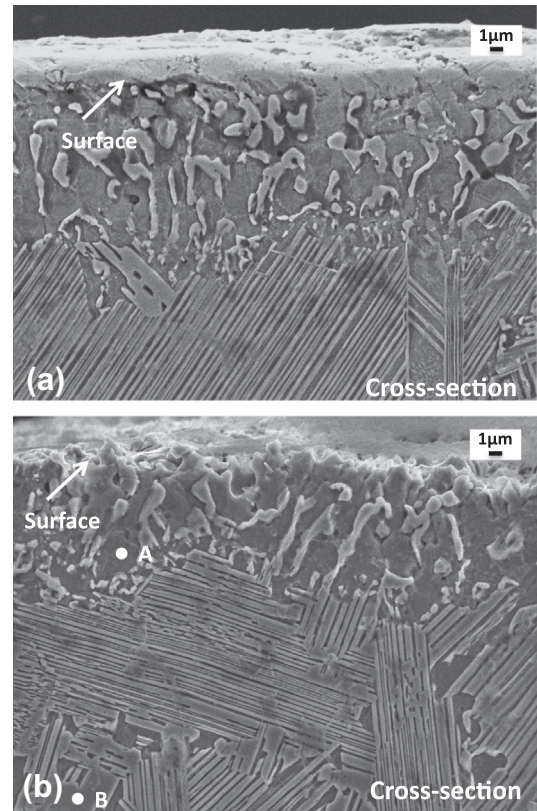


Fig. 8. The cross-sectional SEM images of Hastelloy-B3 (etched) after (a) 500 h and (b) 1000 h of corrosion tests.

distinct structures appeared after corrosion tests; the top layer adjacent to surface of the Hastelloy-B3 is Mo-depleted layer whereas the bottom layer whose composition of Mo is similar to the nominal composition of the matrix, as evidenced by EDX analysis in Table 3. The average depth of the Mo-depleted layer was about 12.38 μm and 12.21 μm for samples tested after 500 h and 1000 h of corrosion test. The compositional distributions from the surface toward the interior region of cross-sectional Hastelloy-B3 after 1000 h of corrosion test are shown in Fig. 9. The surface of Hastelloy-B3 was depleted in Mo; however, no considerable depletion of Cr, Ni and Fe near the surface of the samples was observed. Thus, Mo was the most reactive constituent of Hastelloy-B3 and was selectively attacked when the residual moisture was present in the FLiNaK salts. These results further support Mo is easy to be corroded in the moisture-containing molten salt environments.

In the foregoing, the results of weight loss of the tested alloys show that corrosion rate was reduced after longer hours of immersion under the same residual moisture environments (1.91 wt.%). In addition, the results of chemical compositional distributions in the corroded layers on the surfaces of the alloys indicate that there was a depletion zone of Cr and Mo near the surface of the Hastelloy-N and Hastelloy-B after immersion test of 1000 h, respectively.

Table 3
The compositions of Ni, Cr, Mo and Fe analyzed by EDS in Fig. 8 (wt.%).

EDS point ^a	Ni	Cr	Mo	Fe
A	77.1	1.5	19.0	1.9
B	67.5	1.2	29.3	1.3
Hastelloy-B3	65	1.5	28.5	1.5

^a Points correspond to label in Fig. 8.

As mentioned earlier, the alloys whose constituents have greater negative free energies to form metal fluoride are prone to corrosion. However, corrosion rate of the alloys depends not only on thermodynamic driving force but also on kinetic of the corrosion reactions. Here, we suggest a possible mechanism to explain why corrosion rate was reduced after longer hours of immersion under the same residual moisture environments, as depicted in Fig. 10. At early stage of corrosion test, there was always an adequate supply of constituents available near the surface of tested alloys. Once water or air impurities were present in the FLiNaK salts, the most reactive constituents near the surface (Cr and Mo in this study) were quickly dissolved into molten salt environments through formation of metal fluoride and thus resulted in a significant weight loss of the samples and remarkable corrosion rate. However, when the samples were undergoing longer periods of immersion in the moisture-containing FLiNaK salts, the most reactive constituents near the surface of the samples had been totally consumed and the depletion zones of Cr and Mo were formed in the vicinity of the surface. In other words, with continued dissolution of Cr and Mo during the corrosion tests, the level of concentration of Cr and Mo near the surface of the alloys had fall, which can be supported by the fact that a concentration gradient of Cr and Mo was found on the surface of Hastelloy-N and Hastelloy-B3 after 1000 h of immersion, respectively. Thus, although there still had sufficient residual moisture inside the FLiNaK salts, given that the molten salts were replaced after each test, the dissolution rate was limited by the depletion of Cr and Mo in the vicinity of the surface of the tested alloys and thereby the corrosion rate was reduced. To further dissolve metal elements into FLiNaK salts, the Cr and Mo must migrate outward to the alloy surface and the corrosion rate at the metal surface was in turn controlled by the solid state diffusion from the alloy matrix to the alloy surface. To understand how fast Cr atoms can diffuse in the Ni-based alloys during

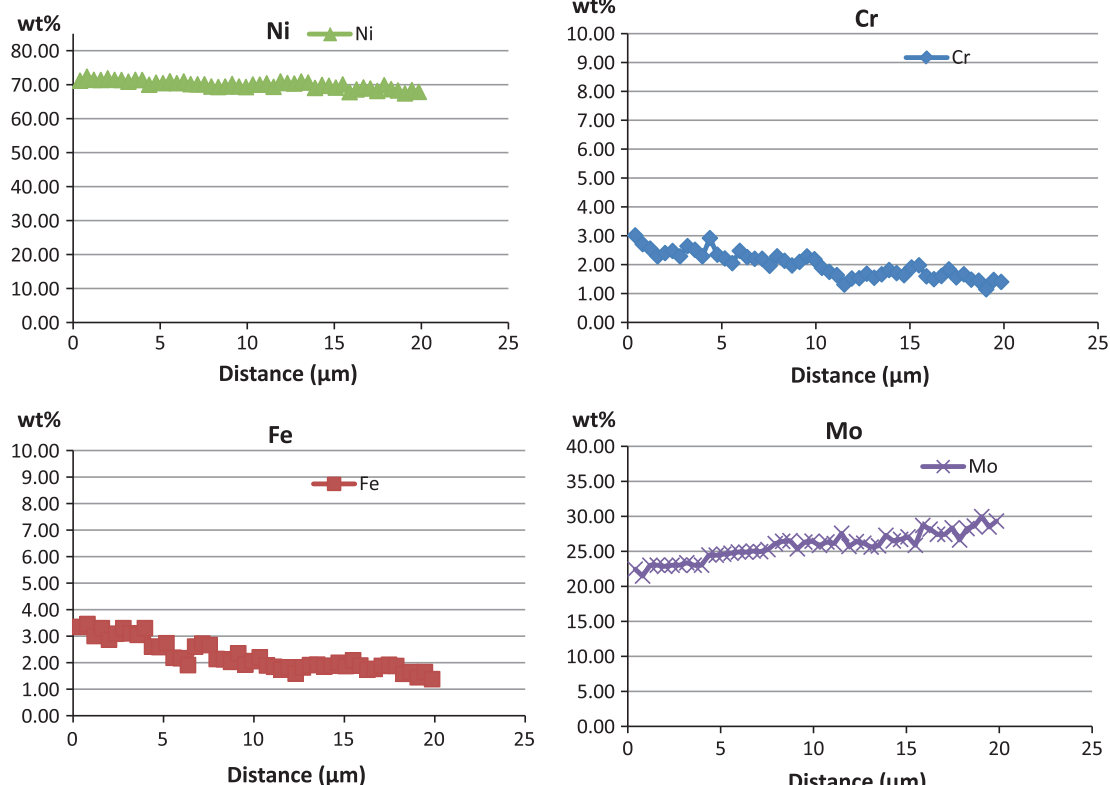


Fig. 9. Compositional distribution of Ni, Cr, Mo and Fe from surface toward the interior of Hastelloy-B3 after 1000 h of corrosion test.

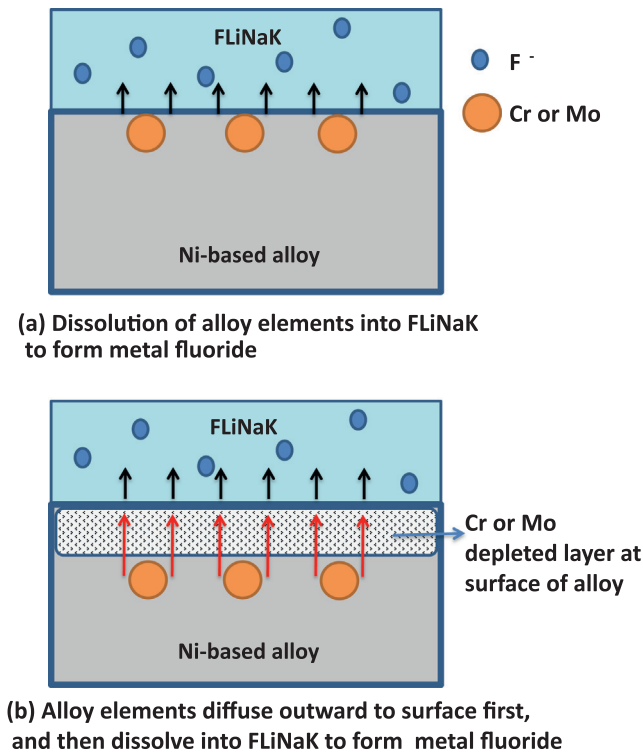


Fig. 10. Schematic diagram of corrosion behaviors of tested alloys at the (a) early and (b) chronic stage of corrosion tests.

In the corrosion test, the diffusion distance of Cr in Ni could be estimated by assuming $x = (Dt)^{1/2}$, where x is the diffusion distance, D is the diffusion coefficient and t is the immersion time. As shown in Fig. 4, corrosion occurred preferentially along grain boundaries at first 100 h and 200 h of corrosion test, inferring that Cr dissolved into the FLiNaK salts through grain boundary diffusion. Based on $\delta D_{gb} = 8.2 \times 10^{-8} \exp(335 \text{ kJ mol}^{-1}/RT)$ [21], grain boundary diffusion coefficient of Cr in Ni-based alloys ($D_{gb,Cr}$) can be calculated as $1.66 \times 10^{-12} \text{ cm}^2/\text{s}$ at 700 °C, where δ is grain boundary width (assume $\delta = 0.5 \text{ nm}$), R is the gas constant and T is the temperature. The diffusion distance of Cr in Ni-based alloys during the period of 100 h would be 7.73 μm; therefore, diffusion rate of Cr in the Ni-based alloys was quite fast and thus led to remarkable corrosion rate at early stage of corrosion tests. In contrast, the corrosion patterns of both alloys tended to be general corrosion at the chronic stage of corrosion tests (Fig. 4), suggesting that Cr and Mo dissolved into the FLiNaK salts through lattice diffusion. Thus, if taking $D_{Cr \text{ in } Ni}$ at 700 °C is $2.51 \times 10^{-15} \text{ cm}^2/\text{s}$, which was calculated based on $D_0 = 1.1 \text{ cm}^2/\text{s}$ and activation energy = 272.6 kJ/mole [22], the diffusion distance of Cr in Ni during the period of 500 h would be 0.67 μm. Similarly, the diffusion distance of Mo in Ni during the corrosion test between 500 h and 1000 h (period of 500 h) is 0.73 μm, given that $D_{Mo \text{ in } Ni}$ at 700 °C is $2.98 \times 10^{-15} \text{ cm}^2/\text{s}$ [23]. These results infer that the diffusion rate of Cr and Mo in the Ni-based alloys is quite slow and this diffusion process is the controlling one. As evidenced in Fig. 8, the depth of the corroded layer of Mo in Hastelloy-B3 only changed slightly after 500 h and 1000 h of immersion. Consequently, the corrosion rates were alleviated for longer hours of immersion, although the residual moisture content in the FLiNaK salts still maintained as 1.91 wt.%. To sum up, the above results suggest that water and air impurities in the FLiNaK salts seemed to dominate the corrosion rate of Hastelloy-N and Hastelloy-B3 at the beginning of the corrosion test; however, once the Cr and Mo near the surface of the alloys were totally dissolved into molten salts, the depletion zones

of Cr and Mo were formed in the vicinity of the surface of the alloys. Cr and Mo must migrate to the alloy surface to sustain attack from the FLiNaK salts. Therefore, the presence of a minor amount of H₂O did not influence the long-term corrosion behavior of tested alloys to a great extent.

4. Conclusions

In this study, we investigated long-term corrosion behaviors of Hastelloy-N and Hastelloy-B3 in moisture-containing molten salt environments at an ambient temperature of 700 °C. Both Hastelloy-N and Hastelloy-B3 exhibited similar weight loss for tested duration of 100–1000 h. The corrosion rates of tested alloys were relatively high at first 100 h and then decelerated rapidly at longer test hours. We proposed that the alleviated corrosion rate may be due to the depletion of the most reactive constituents near the surface of alloys after long-hour immersion and thus the long-term corrosion rate was controlled by the solid state diffusion from the alloy matrix to the alloy surface. A depletion layer of Cr was found near the surface of the Hastelloy-N, whereas a depletion layer of Mo was observed in the vicinity of the surface of the Hastelloy-B3 after 1000 h of immersion. The different behaviors between Hastelloy-N and Hastelloy-B3 may be attributed to the fact that Hastelloy-B3 contained most of Mo in addition to Ni and Mo was easy to be corroded in the moisture-containing molten salts. The results of microstructural characterization revealed that both alloys suffered more intergranular corrosion at early stage of corrosion test, and then experienced general corrosion for longer immersion hours. The results also suggested that the presence of a minor amount of H₂O would enhance corrosion at the early stage, but it would not substantially influence the long-term corrosion performance.

Acknowledgements

We thank National Science Council of Taiwan, ROC, for financial support under Contract Nos. NSC98-3114-Y-007-001 and 102-3113-P-007-014.

References

- [1] D.F. Williams, Assessment of Candidate Molten Salt Coolants for the NGNP/NHI Heat-Transfer Loop, Oak Ridge National Laboratory, ORNL/TM-2006/69, 2006.
- [2] D.F. Williams, Assessment of Candidate Molten Salt Coolants for the Advanced High-Temperature Reactor (AHTR), Oak Ridge National Laboratory, ORNL/TM-2006/12, 2006.
- [3] D. Williams, D. Wilson, J. Keiser, L. Toth, J. Caja, Am. Nucl. Soc. Winter Meet. 2003 (2003) 1–12.
- [4] J. Koger, in: S. Cramer, B. Covino (Eds.), Corrosion: Fundamentals, Testing, and Protection, ASM Handbook, vol. 13A, ASM International, OH, 2003, pp. 124–128.
- [5] L.C. Olson, J.W. Ambrosek, K. Sridharan, M.H. Anderson, T. Allen, J. Fluorine Chem. 130 (2009) 67–73.
- [6] L.C. Olson, K. Sridharan, M. Anderson, T. Allen, J. Nucl. Mater. 411 (2011) 51–59.
- [7] W. Manly, J. Coobs, J. DeVan, D. Douglas, H. Inouye, P. Patriarca, T. Roche, J. Scott, in: R. Hurst, R.N. Lyon, C.M. Nicholls (Eds.), Progress in Nuclear Energy, Series IV: Technology, Engineering and Safety, vol. 2, Pergamon Press, New York, 1960, pp. 164–179.
- [8] J. Steinmetz, P. Steinmetz, A. Huntz, Solid State Phenom. 21 (22) (1992) 223–276.
- [9] M. Kondo, T. Nagasaka, V. Tsisar, A. Sagara, T. Muroga, T. Watanabe, T. Oshima, Y. Yokoyama, H. Miyamoto, E. Nakamura, N. Fuji, Fusion Eng. Des. 85 (2010) 1430–1436.
- [10] M. Kondo, T. Nagasaka, Q. Xu, T. Muroga, A. Sagara, N. Noda, D. Ninomiya, M. Nagura, A. Suzuki, T. Terai, N. Fujii, Fusion Eng. Des. 84 (2009) 1081–1085.
- [11] C.F. Weaver, H.A. Friedman, A Literature Survey of Fluorides and Oxyfluorides of Molybdenum, Oak Ridge National Laboratory, ORNL-1976, 1967.
- [12] J.W. Koger, Mass Transfer between Hastelloy N and Alloy No. 25 in a Molten Sodium Fluoborate Mixture, Oak Ridge National Laboratory, ORNL-3488, 1971.

- [13] R.E. Thoma, Phase Diagrams of Nuclear Reactor Materials, Oak Ridge National Laboratory, ORNL-2548, 1959.
- [14] V. Kirillov, V. Fedulov, Translated from Fiziko-Khimcheskaya Mekhanika Materialov, 16(6) (1980) 22–25.
- [15] Manohar S. Sohal, Matthias A. Ebner, Piyush Sabharwall, Phil Sharpe, Engineering database of liquid salt thermophysical and thermochemical Properties, Idaho National Laboratory, INL/EXT-10-18297, 2010.
- [16] W.F. Gale, T.C. Totemeier, Thermochemical data, in: Smithells Metals Reference Book, Elsevier Butterworth-Heinemann, 2004, pp. 24–26.
- [17] C.J. Tyreman, The High Temperature Corrosion of Metals and Alloys in HF-containing Environments, PhD thesis, University of Manchester, Manchester, UK, 1986.
- [18] F.-Y. Ouyang, C.-H. Chang, B.-C. You, T.-K. Yeh, J.-J. Kai, J. Nucl. Mater. 437 (2013) 201–207.
- [19] J.W. Koger, Corrosion And Mass Transfer Characteristics of NaBF₄-NaF(92-8 mole %), in: Hastelloy N, Oak Ridge National Laboratory, ORNL-3866, 1972.
- [20] R.E. Gehlbach, H.E. McCoy Jr., Phase instability, in: Hastelloy N, in: international symposium on structural stability in superalloys, 1968, pp. 346–366.
- [21] Tien-Fu Chen, Gyanendra Prasad Tiwari, Yoshiaki Iijima, Kiyoshi Yamauchi, Mater. Trans. 44 (1) (2003) 40–46.
- [22] R.L. Gruzin, S.V. Zemskii, I.B. Rodina, Metallurgy and Metallography of Pure Metals, No. 4. Moscow, 1963, 243, (AERE Trans. 1032).
- [23] C.E. Campbell, W.J. Boettinger, U.R. Kattner, Acta Mater. 50 (2002) 775.